**Computers and Chemical Engineering** 

Special Issue on Decarbonization and Circular Economy

Deadline for manuscript submission: April 2025

A Mathematical Programming Model for the Optimal Utilization of Deep Saline Aquifers for CO<sub>2</sub> Storage

Diego J. Trucco<sup>a,b</sup>, Demian J. Presser<sup>a,b</sup>, Diego C. Cafaro<sup>a,b</sup>, Ignacio E. Grossmann<sup>c</sup>, Saurabh Shenvi Usgaonkar<sup>d</sup>, Qi Zhang<sup>d</sup>, Pratik Misra<sup>d</sup>, Heather Binagia<sup>d</sup>, Wayne Rowe<sup>d</sup>, Sanjay Mehta<sup>d</sup>

<sup>a</sup>INTEC (UNL-CONICET), Santa Fe, Argentina.

<sup>b</sup>Facultad de Ingeniería Química, Universidad Nacional del Litoral, Santa Fe, Argentina

<sup>c</sup>Department of Chemical Engineering, Carnegie Mellon University, Pittsburgh, Pennsylvania, United States

<sup>d</sup>Air Products and Chemicals Inc., Allentown, Pennsylvania, United States

**Abstract** 

This work presents a novel nonlinear programming (NLP) formulation aimed at maximizing the overall amount of CO<sub>2</sub> stored into deep saline aquifers in the long term. The goal is to optimally determine CO<sub>2</sub> injection rates into vertical wells while properly managing bottom-hole pressures over time. The reservoir may comprise several layers with heterogeneous physical properties. The injection plan should meet the subsurface engineering policies for safe operations along with existing technical constraints. The major challenge is to track the CO<sub>2</sub> migration across the reservoir to ensure containment during the injection periods and also in the long term. The NLP formulation is based on a discrete space and time representation of the reservoir, comprising pressure propagation and mass balance equations between every pair of adjacent blocks in the grid. Results for several illustrative case studies in two dimensions show the potential of the model to find optimal solutions in few seconds. Injection plans suggested by the optimization model are efficient and have been validated by accurate simulation runs. Based on these findings, the model has the potential to be extended to three dimensions and adapted to real-world cases.

Introduction

There is international scientific consensus that anthropogenic emissions of carbon dioxide (CO<sub>2</sub>) need to fall dramatically by 2030 if the aim is to eventually reach net zero around 2050. Achieving net zero emissions by 2050 is an ambitious target that will require large-scale deployment of carbon capture, utilization, and storage technologies (CCUS) (Air Products, 2024). It is essential to develop technically sound, safe, and cost-effective CO<sub>2</sub> injection and well operation strategies. This involves a sophisticated balance of various factors such as subsurface engineering, technical constraints, and

1

economic trade-offs. Optimization techniques are the best tools to manage this complexity and ensure that CCUS projects are economically viable, while maintaining safety and environmental standards. (Ismail and Gaganis, 2023).

For underground storage, companies frequently target deep saline formations and depleted oil and gas fields (Pires et al., 2011). Saline formations are characterized by porous rock matrices saturated with brine (over 10,000 ppm salinity), which are favored for their vast storage capacity and widespread geographic availability. Estimates suggest that the U.S. possesses between 3,000–6,000 gigatons of storage capacity, with deep saline formations accounting for over 97–99% of this potential (US Geological Survey, 2013). The porous rock layer typically features high-permeability sandstone or limestone that facilitate CO<sub>2</sub> injection and storage, overlaid by a low-permeability caprock, which acts as a geological containment that seals in the CO<sub>2</sub>. These storage formations often extend laterally for many miles and are located more than 800 m below the surface, safely beneath fresh groundwater deposits. At such depths, CO<sub>2</sub> remains in supercritical state, with temperatures exceeding 50°C and pressures above 10 MPa, with a density around 600 kg/m³ (Zou and Durlofsky, 2023). Under these conditions, it behaves as a dense fluid, occupying less space in the reservoir and thereby enhancing storage efficiency.

The storage of CO<sub>2</sub> into deep saline aquifers mostly occurs at natural formation pressures. Reservoirs are generally represented as open systems from which the brine can flow laterally, and make room for the injected CO<sub>2</sub> that is trapped in the porous media (Nordbotten et al., 2005). Although pressure build-up is not as relevant as for closed systems (e.g., depleted oil and gas reservoirs), pressure signals during injection can propagate far beyond the CO<sub>2</sub> migration front ("plume"), on the scale of tens to even hundreds of kilometers (Birkholzer et al., 2015). Continuous measurement, monitoring, verification, and reporting during sequestration must be carefully recorded by companies, requiring sophisticated simulation and optimization tools to make proper decisions. In practice, operators often rely on empirical correlations and over-simplified extrapolation techniques to estimate CO<sub>2</sub> sequestration capacities, and it is even more challenging to estimate the extent of CO<sub>2</sub> retention, leakage, and spread within the reservoir over time (Hasan et al., 2022).

This work presents a novel mathematical programming model for the optimal planning of CO<sub>2</sub> injection into deep saline aquifers, aiming at maximizing overall carbon sequestration in the long term. We introduce a Nonlinear Programming (NLP) formulation based on a discrete space-time representation of the reservoir, which is initially saturated with brine. The storage aquifer is assumed to be heterogeneous, made up of multiple layers, and each block in the grid is characterized by specific permeability and porosity estimations. CO<sub>2</sub> injection into the reservoir is performed through multiple

vertical wells whose geographical location and depth are given a priori. The prediction of reservoir pressure gradients and CO<sub>2</sub> migration is proposed with simplified models to solve the optimization problem by means of mathematical programming tools rather than using sampling and metaheuristic strategies as has been reported in the literature (Cameron and Durlofsky, 2012; Sun and Dusrlofsky, 2019). More specifically, we seek to overcome limitations of previous contributions in the field that require numerous simulations and do not guarantee optimality after very long time computations.

Compared to metaheuristics, mathematical programming benefits by the inclusion of boundary constraints, such as CO<sub>2</sub> containment. While the former usually treat such constraints using penalty functions and repair procedures, active set solvers for very large nonlinear programming (NLP) models take advantage by searching along a feasible path, tight at the boundary. See Biegler (2010) for a general review on NLP algorithms. Most active set, feasible path methods are based on the generalized reduced-gradient (GRG) algorithm proposed by Abadie and Carpentier (1969), and more recent extensions by Drud (1996), which generally perform better when solving models with many equality constraints (mostly linear) and few bounds, like the model developed in this paper. The feasibility of the intermediate points, satisfying thousands of material and pressure balances is carefully preserved.

However, the development of a proper prediction model of reasonable dimensions for optimization purposes is challenging. To build the model we rely on a discrete space-time representation, much coarser than typical simulation models, including material balances and Darcy's law equations (Darcy, 1856) to track the CO<sub>2</sub> front over time. Buoyancy effects are also modeled with detail due the significant difference of densities between water and supercritical CO<sub>2</sub> (Celia et al., 2015). Finally, dynamic pressure propagation curves are also predicted from Darcy's law applied to multiphase flows, evaluating changes along the horizontal and vertical dimensions of the system.

The primary objective of this paper is to present the foundation of a mathematical programming model capable of guiding operators in designing optimal CO<sub>2</sub> injection strategies for multiple vertical wells. The aim is to address the most critical trapping mechanisms and transportation phenomena while maintaining computational efficiency.

### **Previous works**

Numerous studies have demonstrated that managing well injection greatly influences how the CO<sub>2</sub> plume extends into reservoirs, as it affects the interplay of natural forces that govern this process (Kumar, 2007; Shamshiri & Jafarpour, 2010). Difference of densities between the bulk phases leads to gravitational forces that drive the CO<sub>2</sub> upward, towards the caprock. This retention mechanism is

known as stratigraphic or structural trapping, and is regarded as the least reliable because the CO<sub>2</sub> remains mobile and may eventually surpass licensed region boundaries (Cameron & Durlofsky, 2012; Massarweh & Abushaikha, 2024). Increasing the injection rate enhances viscous forces, resulting in a flatter and more uniform CO<sub>2</sub> front. This facilitates horizontal movement, broadens the CO<sub>2</sub> plume, and increases its interaction with brine. Such strategies promote solubility trapping (a fraction of the CO<sub>2</sub> being dissolved in the brine), and residual trapping, which occurs due to hysteresis effects driven by capillary pressure and the relationship between relative permeability and saturation of the involved phases (Weir et al., 1995).

Many of these features are thoroughly reviewed by Kumar (2007), widely regarded as a pioneer in the application of optimization tools to CO<sub>2</sub> sequestration. In this seminal work, the author leverages advanced optimization techniques already established in other areas of reservoir engineering, particularly in oil recovery operations such as waterflooding (Yeten et al., 2002). Using the conjugate gradient method, the author seeks for the injection strategy that maximizes the proportion of CO<sub>2</sub> stored through residual trapping, given a total amount of CO<sub>2</sub> to be injected. The objective function is evaluated using a commercial numerical reservoir simulation (NRS) model. Based on successive evaluations, gradients can be estimated using finite differences, which guide adjustments to the control variables (valve settings). However, the algorithm is likely to converge to local optima, particularly when the permeability distribution is highly heterogeneous. For this reason, multiple optimization paths, each with a different starting point, are suggested to increase the likelihood of identifying the actual optimum. Needless to say, a very large number of simulations are required.

Kumar (2007) advocates for the development of an integrated method to optimize the CO<sub>2</sub> sequestration process. Such approach could overcome the inherent "black-box" nature of commercial simulators, which hinders the precise determination of gradients. Nevertheless, subsequent researchers have continued to favor simulation-based optimization (SBO), wherein the optimization process is conducted iteratively, based on previous simulation results. Simulation and optimization steps are repeated until convergence to a near optimal solution. The optimization approach may involve gradient-based or derivative-free methods. While the former are generally recommended due to their stronger convergence, SBO often encounters challenges in obtaining the necessary derivative information, as an interface with the source code needs to be available. This limitation persists even when the objective function and constraints are smooth (Kolda, 2003).

Shamshiri and Jafarpour (2010) employ the quasi-Newton BFGS method (Nocedal & Wright, 2006) to enhance the sweep efficiency of the CO<sub>2</sub> plume within the reservoir. The authors reaffirm that injection strategies can influence CO<sub>2</sub> movement within the reservoir, encouraging a more uniform

front despite reservoir heterogeneities. Similarly, Cameron and Durlofsky (2012) aim to minimize the mobile fraction of CO<sub>2</sub> to reduce the risk of leakage. In contrast to the previous studies, they apply the Hooke-Jeeves Direct Search (HJDS) method (Hooke & Jeeves, 1961), a derivative-free optimization technique. However, the absence of gradient information increases the number of function evaluations compared to gradient-based approaches. Consequently, hundreds or even thousands of simulations are required. Finally, the authors propose hybridizing HJDS with probabilistic search algorithms to improve the robustness of the framework. In a similar line, Zhang and Agarwal (2012) develop a genetic algorithm coupled with the multiphase numerical solver TOUGH2 (Doughty, 2013) to improve CO<sub>2</sub> storage efficiency while simultaneously reducing plume extension.

More recently, Zou and Durlofsky (2023) test the efficacy of two metaheuristic approaches to solve this problem, namely Particle Swarm Optimization (PSO) (Kennedy & Eberhart, 1995) and Differential Evolution (DE) (Storn & Price, 1997), to determine both well placement and injection rates. Metaheuristics guide the optimization process toward regions of interest within the search space based on a predefined criterion (fitness function). Due to their probabilistic nature, metaheuristics cannot guarantee convergence to the optimum within a finite time, but they are generally more likely than other derivative-free methods to identify high-quality solutions (Yang, 2010). However, metaheuristics require a large number of function evaluations, particularly when the number of decision variables is large and of continuous nature. To reduce the effort, Zou and Durlofsky (2023) propose a multi-fidelity approach, with three levels of grid resolution.

Data-driven modeling (DDM) is a more recent alternative to traditional NRS. These models are trained using data generated by numerical simulations to eventually predict the responses of the reservoir, while achieving execution times of just a few seconds (Zhang & Sahinidis, 2013; Ng et al., 2023). Surrogate or proxy models are employed to guide metaheuristics toward the improvement of the value function. If a high-fidelity proxy model is successfully developed, decision-making processes can be significantly faster. However, training these models is inherently complex and time-consuming. Furthermore, even after a surrogate model has been properly trained and validated, its predictive accuracy may fail to generalize effectively to different reservoir characterizations. For that reason, the DDM paradigm is predominantly applied to CO<sub>2</sub> injection into depleted oil fields (You et al., 2020; Vo et al., 2020; Sun et al., 2021, Abhijnan et al., 2024) where a substantial amount of data is typically available from previous production phases. Instead, CO<sub>2</sub> injection into deep saline aquifers faces significant challenges due to the inherent uncertainty in reservoir properties (Miller et al., 2014).

Interestingly, the simplified representation of reservoir dynamics by means of proxy models enables the development of integrated simulation-optimization frameworks. These surrogate models can be embedded as sets of linear or nonlinear equations within the mathematical formulation, depending on the prediction method. For instance, Borda et al. (2017) analyze various methods for predicting reservoir pressures to optimize CO<sub>2</sub> injection into the Nelson Field reservoir (Arizona, United States). The optimization model accounts for key constraints, such as mitigating pressure build-up to preserve reservoir integrity. Unlike metaheuristics, this framework seeks for the optimal solution while strictly satisfying the constraints, provided that the surrogate models achieve sufficient predictive accuracy. Nonetheless, this approach is limited to a single geophysical variable: pressure. Expanding the scope to control multiple variables across broader domains introduces substantial complexity to train surrogate models. This undermines computational efficiency and can also degrade the accuracy.

In contrast to all previous contributions, this work presents a novel mathematical programming model for the optimal planning of CO<sub>2</sub> injection into deep saline aquifers through multiple wells as an integrated simulation-optimization framework based on first-principle equations. To the best of our knowledge, this optimization approach is the first to incorporate physics-informed equations to predict complex, non-linear system evolution. In contrast to previous methods, this framework overcomes the reliance on external numerical simulations and surrogate models.

### **Motivation**

Mathematical programming emerges as a promising alternative to simulation-based optimization methods. Constraints related to subsurface engineering and regulatory policies, such as pressure management and CO<sub>2</sub> containment, can be incorporated directly into the model to ensure safe conditions. This can also help solvers narrow the search space and provide valuable guidance in derivative information. In contrast to metaheuristics and data-driven approaches, we argue that a physics-informed model can better exploit the advantages of mathematical programming, also leveraging interpretability. While the underlying system dynamics in reservoir simulation are inherently complex (Voskov et al., 2017), simplifications can be introduced to represent the physics without compromising accuracy to an unacceptable degree (Celia et al., 2015).

In this initial study, our objective is to capture the key reservoir dynamics to maintain the practical applicability of the model for optimization purposes. By doing so, we aim to highlight the potential of mathematical programming to address challenges in CO<sub>2</sub> injection planning and reservoir management. However, as shown later in this work, NRS will still play a crucial role to validate injection plans with more accuracy.

## **Problem statement**

The optimization problem addressed in this work can be stated as follows. Given are the following items:

- (a) A deep saline aquifer with uniform width (dimension y), known extension (dimension x) and depth (dimension z), to be used for carbon sequestration, also called the control volume.
- (b) A set of different layers in the z dimension of the reservoir where  $CO_2$  migration and trapping mechanisms occur.
- (c) A set of vertical wells with known location, comprising one or multiple injection points at different layers into which carbon dioxide can be pumped in for storage.
- (d) Reservoir characterization (permeability, porosity, saturation map and pressure constraints) all across the control volume.
- (e) A set of time periods comprising a multi-year planning and control horizon.
- (f) Maximum amount of CO<sub>2</sub> flow available for injection in each time period.

The goal is then to determine the optimal multi-well injection plan that maximizes the total amount of CO<sub>2</sub> stored in the long-term, given in terms of injection rates and bottom-hole pressures at each well along the time horizon. The aim is to predict pressure propagation during injection and CO<sub>2</sub> migration in the long-term to comply with injectivity and containment constraints.

### **Model assumptions**

The design of a model that effectively balances computational efficiency with predictive accuracy poses significant challenges. The model proposed in this work predicts the reservoir behavior over time by means of a system of nonlinear algebraic equations and constraints. To build the model we make the following assumptions:

- a) For simplicity, the reservoir is represented by a 2D grid-based model (dimension *x* for length and *z* for depth) so that the width (dimension *y*) of every block is fixed (see Fig. 1). Although this assumption does not necessarily fit real-world reservoirs, it permits to setup a primary optimization model that can be easily understood and eventually be extended to 3D. Extensions to 3D will be addressed in a forthcoming article.
- b) The reservoir is covered with a zero-permeability caprock, which acts as a structural containment that prevents the CO<sub>2</sub> to flow to the surface. At the bottom of the deep-most layer permeability is also assumed to drop to zero.
- c) Porous space of any block in the reservoir can be occupied with only two components: CO<sub>2</sub> and brine. At the reservoir conditions, CO<sub>2</sub> is in supercritical state. For simplicity, it is assumed that

- brine and CO<sub>2</sub> have constant densities across the reservoir at any time period. Furthermore, miscibility and thermodynamic phenomena are omitted, for simplicity.
- d) Mass transport properties of fluids (e.g., viscosity, density) and reservoir blocks (e.g., porosity, permeability, effective permeability) are explicitly included in the model.
- e) For CO<sub>2</sub> flow prediction, Darcy's law is utilized based on saturation and pressure differences between adjacent grid blocks.
- f) Dynamic pressure propagation can be also modeled through Darcy's law for multiphase flows, based on average properties including rock permeability and fluid viscosity.
- g) Injection management is performed through continuous variables only, with all equations formulated in quadratic form, yielding a quadratically constrained program (QCP).
- h) Actual relative permeability curves, derived from experimental data, are included in the model in the form of fourth order polynomial equations.
- i) The reservoir is assumed to be open in the *x* dimension, from which a pseudo-open system representation is adopted. The number of blocks in the *x* dimension (columns) is finite, but those blocks at the boundaries are treated in a particular manner. They can steadily receive material from adjacent blocks within the control volume without building-up pressure. In other words, they are considered as having an infinite volume at a constant pressure (the reservoir pressure).
- j) Only residual and structural trapping mechanisms are accounted for. Since the time horizon spans for few decades, mineral trapping is excluded from the analysis. Solubility trapping is also omitted for simplicity. From experimental analysis, CO<sub>2</sub> solubility is usually below 50 g per kg of brine at reservoir conditions (Massarweh & Abushaikha, 2024). Nevertheless, we plan to extend the model to account for CO<sub>2</sub> solubility in future works.

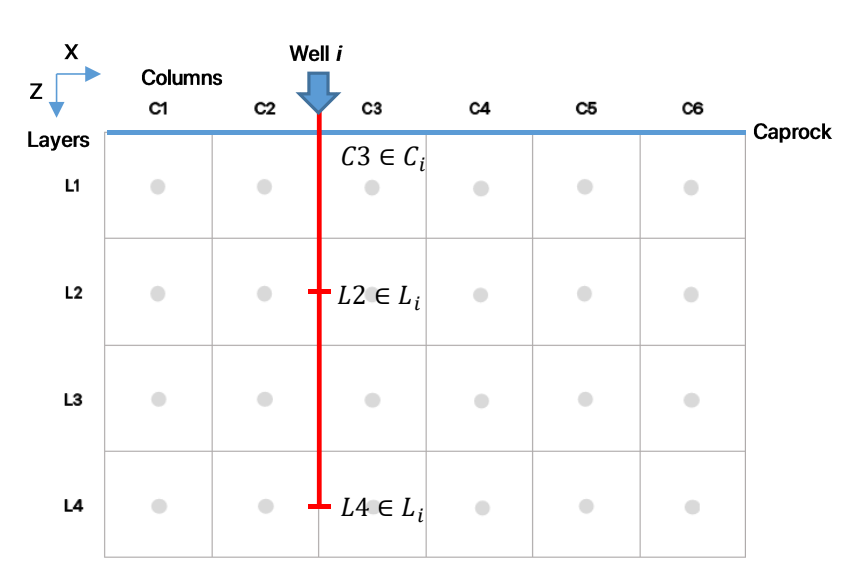


Fig. 1. Two-dimensional grid representation of the reservoir.

## **Mathematical formulation**

This section presents the first Nonlinear Programming (NLP) mathematical formulation aimed at maximizing the total amount of  $CO_2$  injected through multiple wells into a deep saline aquifer to be safely stored in the long term. The model is fully discretized in space and time domains, with indices c and l standing for columns and layers, and t for time periods, respectively. Injection wells are identified with the index i.

The constraints included in the model can be divided into two main categories: (i) those designed to model the evolution of the reservoir over space and time, accounting for pressure propagation and CO<sub>2</sub> migration, and (ii) those dealing with operational limitations of the injection process itself, ensuring safe and long-term containment of the CO<sub>2</sub> while maintaining reservoir integrity. The former are usually given in terms of equalities (e.g., mass balances), while the latter are bound constraints in the form of lesser-or-equal inequalities (e.g., maximum saturation).

## **Balance equations**

Regarding reservoir dynamics, it is assumed that the reservoir starts fully saturated with brine. Saturation is an important state variable of every block (c, l) that needs to be tracked over time. It stands for the fraction of a certain component (CO<sub>2</sub> or brine) relative to the total porous space. By assumption, the miscible fraction of CO<sub>2</sub> into brine (solubility trapping) is omitted for simplicity.

Under these assumptions, Darcy's law (1856), as presented in Eq. 1, can be adapted to predict pressure gradients and/or fluid flowrates in terms of finite difference equations. This is achieved by averaging the physical properties of the fluids across the reservoir, yielding good estimations of the pressure and flow variables. The volumetric flow rate Q is a function of the permeability of the porous medium (k), the viscosity of the fluid  $\mu$  and the pressure gradient  $\nabla P$ . Consistent with its physical interpretation, higher permeability enhances fluid mobility within the medium, whereas viscosity has the opposite effect. Lastly, a reduction in the magnitude of the pressure gradient directly reduces the flowrate,

$$Q = -\frac{k}{\mu} \nabla P \tag{1}$$

### Tracking pressures

To account for pressure variations across the reservoir, we introduce the concept of dynamic pressure (DP) defined as the pressure increase (above static pressure sp) caused by well injection. Dynamic pressure propagates throughout the reservoir, such that the total pressure  $P_{c,l,t}$  at a given block (c, l)

is the sum of the static pressure of layer l (given data) and the net dynamic pressure projected from all injection points into layers  $l' \in L_i$  along every well i. That summation is presented in Eq. 2,

$$P_{c,l,t} = sp_l + \sum_{i \in I} \sum_{l' \in L_i} DP_{c,l,t}^{(i,l')} \qquad \forall c \in C, l \in L, t \in T$$
 (2)

Without loss of generality, we assume that the dynamic pressure driven by  $CO_2$  pumping will dissipate along  $n_{diss}$  blocks horizontally, which can be estimated from prior geological studies. Given that the system representation is based on a pseudo-open domain, this parameter can be adjusted when boundary blocks are reached. The complete dissipation of dynamic pressure is enforced by Eq. 3. Note that column  $c \in C_i$  determines the well location along dimension x.

$$DP_{c',l,t}^{(i,l)} = 0 \qquad \forall i \in I, l \in L_i, c \in C_i, c' \notin [c - n_{diss}, c + n_{diss} - 1], t \in T$$
 (3)

*CO*<sup>2</sup> *injection flow according to the bottom-hole pressure* 

To estimate the amount of  $CO_2$  directly injected into a block (c, l) adjacent to the injection point at layer  $l \in L_i$  (denoted by  $QT_{i,c,l,t}$ ) we rely on Darcy's law applied to a system of resistors in series along every injection layer (see Fig. 2). This is applied for each direction, i.e. to the right (column c) and to the left (column c - 1) of the injection point, with well i placed at the left of column  $c \in C_i$ . As expressed by Eqs. 4 and 5, the injection flow rates to the right and to the left, respectively, can be estimated from the bottom-hole pressure BHP, reservoir permeability  $kh_{c,l}$  and average viscosity  $\mu avg_{c,l,t}$  across the series of  $n_{diss}$  blocks in the corresponding direction. Analogously to an electric circuit, resistance (inverse of conductance) of subsequent blocks are summed along each horizontal direction. As illustrated in Fig. 2, a higher  $CO_2$  saturation yields a lower viscosity, resulting in smaller pressure drops. Note that, by convention, the BHP of any well is measured at the same depth ( $depth_o$ , of layer l1), given that there may be multiple injection points along the vertical well.

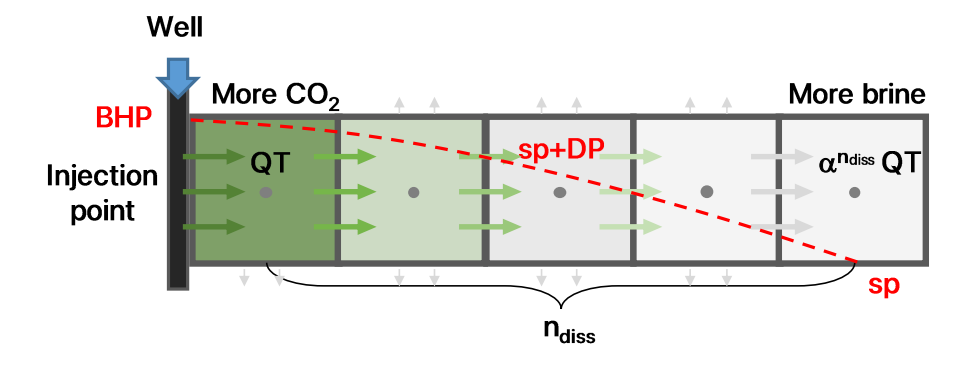


Fig. 2. Dynamic pressure propagation and CO<sub>2</sub> migration in the horizontal direction, to the right of an injection point.

$$QT_{i,c,l,t} = \frac{BHP_{i,t} + \rho_{CO2} \ g \ (depth_l - depth_o) - sp_l}{\sum_{c'=c}^{c+n} diss^{-1} \alpha^{c'-c} \ kh_{c',l}^{-1} \ length \ area^{-1} \ \mu avg_{c',l,t}} \qquad \forall i \in I, c \in C_i, l \in L_i, t \in T$$
 (4)

$$QT_{i,c-1,l,t} = \frac{BHP_{i,t} + \rho_{CO2} \ g \ (depth_l - depth_o) - sp_l}{\sum_{c'=c-n_{diss}}^{c-1} \alpha^{c-1-c'} \ kh_{c',l}^{-1} \ length \ area^{-1} \ \mu avg_{c,l,t}} \qquad \forall i \in I, c \in C_i, l \in L_i, t \in T$$
 (5)

For accuracy, an adjustment factor  $\alpha$  slightly smaller than one is incorporated in the model to account for the flow diversion in the vertical direction. More specifically, from the incompressibility assumption, the total amount of CO<sub>2</sub> injected to the right  $(QT_{i,c,l,t})$  will reduce to  $\alpha^n$   $QT_{i,c,l,t}$  volume units of a multiphase fluid (brine + CO<sub>2</sub>), n blocks at the right of the injection point.

As stated in Eq. 6, the average viscosity of the multiphase fluid is roughly calculated by weighting the individual viscosities according to the CO<sub>2</sub> saturation  $S_{c,l,t}$  at block (c, l) at time t,

$$\mu avg_{c,l,t} = \mu_{CO_2} S_{c,l,t} + \mu_{brine} \left( 1 - S_{c,l,t} \right) \qquad \forall c \in C, l \in L, t \in T \quad (6)$$

Finally, the total injection into well i over period t, represented by the variable  $Y_{i,t}$ , can be calculated as in Eq. 7, summing  $CO_2$  flows towards both directions, over all injection layers,

$$Y_{i,t} = \sum_{l \in L_i} \left( QT_{i,c-1,l,t} + QT_{i,c,l,t} \right) \qquad \forall i \in I, c \in C_i, t \in T$$
 (7)

Pressure propagation in the horizontal direction

To estimate the propagation of dynamic pressures along injection layers, the finite-difference form of Darcy's law (1856) in Eq. 1 is applied to adjacent blocks, based on the previously computed total flow rate  $QT_{i,c,l,t}$ . Eqs. 8 and 9 account for pressure drops along adjacent blocks, in both horizontal directions (i.e., to the right and to the left, respectively),

$$DP_{c,l,t}^{(i,l)} = DP_{c-1,l,t}^{(i,l)} - \frac{\alpha^{c-c'} QT_{i,c',l,t} \ length \ \mu avg_{c,l,t}}{kh_{c,l} \ area}$$
(8)

$$\forall i \in I, l \in L_i, c' \in C_i, c \in C: c > c', t \in T$$

$$DP_{c-1,l,t}^{(i,l)} = DP_{c,l,t}^{(i,l)} - \frac{\alpha^{c'-1-c} QT_{i,c'-1,l,t} \ length \ \mu avg_{c,l,t}}{kh_{c,l} \ area}$$
(9)

$$\forall i \in I, l \in L_i, c' \in C_i, c \in C: c < c' - 1, t \in T$$

For blocks adjacent to injection points, where  $CO_2$  is directly injected, one may also assume a horizontal pressure drop provoked by half of the length of the corresponding block, assuming that pressures are measured at the center of each element (c, l). Hence, to calculate the pressure gradient

necessary to reach the center of those blocks, Eq. 10 can be incorporated into the model. For clarity, Fig. 2 also provides a visual interpretation of the pressure gradient.

$$DP_{c,l,t}^{(i,l)} = BHP_{i,t} + \rho_{CO2} g \left( depth_l - depth_o \right) - sp_l - \frac{QT_{i,c,l,t} \ length/2 \ \mu avg_{c,l,t}}{kh_{c,l} \ area}$$
 (10)

$$\forall i \in I, l \in L_i, c' \in C_i, c = c', c' - 1, t \in T$$

Pressure propagation in the vertical direction

To further refine the modeling of dynamic pressure propagation to different layers within the reservoir, we take the reference pressure at each column of the injection layer l' (variable  $DP_{c,l',t}^{(i,l')}$ , obtained from Eqs. 8, 9 and 10) and assume a geometric dissipation in both directions along the vertical axis. More specifically, dynamic pressure is assumed to reduce by a factor of  $\frac{\mu_{brine}}{\mu avg_{c,l,t}} \frac{kv_{c,l}}{kh_{c,l}}$  every time we move a layer up or down from the injection layer. As stated in Eqs. 11 and 12, respectively,

$$DP_{c,l-1,t}^{(i,l')} = DP_{c,l,t}^{(i,l')} \frac{\mu_{brine}}{\mu avg_{c,l,t}} \frac{kv_{c,l}}{kh_{c,l}}$$
(11)

$$\forall c \in C, i \in I, l' \in L_i, l \leq l', t \in T$$

$$DP_{c,l+1,t}^{(i,l')} = DP_{c,l,t}^{(i,l')} \frac{\mu_{brine}}{\mu avg_{c,l,t}} \frac{kv_{c,l}}{kh_{c,l}}$$
(12)

$$\forall c \in C, i \in I, l' \in L_i, l' < l, t \in T$$

Note that the factor  $kv_{c,l}/kh_{c,l}$  is the relationship between the vertical and horizontal permeability of the block (c, l), which in practice is usually small (in the order of  $10^{-2}$ ). Besides, dissipation is smoother if the fluid contained by the block is less viscous. From Eq. 6, the factor  $\mu_{brine}/\mu avg_{c,l,t}$  satisfies  $1 \le \mu_{brine}/\mu avg_{c,l,t} \le (1 - s_{max})^{-1} \approx 5$ . Hence,  $DP_{c,l,t}^{(i,l')}$  typically reduces from 20 to 100 times per block in the vertical direction (depending on the saturation), rapidly going to zero and favorably comparing to simulation experiments. Also note that nonlinear Eqs. 11 and 12 can be written to preserve the bilinear, quadratic form since  $\mu avg_{c,l,t}$  is a linear function of  $S_{c,l,t}$ .

### Extra pressure due to buoyancy at the top layer

Since the top layer of the reservoir (namely l1) is assumed to lie beneath an impermeable rock formation, it is necessary to include an extra term for buoyancy pressure  $BP_{c,l1,t}$  at the columns of that particular layer. This term is added to accurately account for the upwards forces exerted by  $CO_2$  (typically lighter than brine) when reaching the caprock. In other words, buoyancy pressure arises at

the top layer due to the difference of densities between the components and plays a critical role in modeling vertical pressure gradients. In particular, it is important to evaluate the stability of the reservoir (maximum saturation) and the typical distribution of  $CO_2$  in the form of an inverted "cone" in the very long term. To incorporate this effect, Eq. 2 is rearranged as shown in Eq. 13. The estimation of buoyancy pressure is directly related to saturation of the blocks below (c, l1). As described in Eq. 14, this relationship is expressed as a weighted summation, where the weights  $\delta_l$  decrease with l and can be fitted to the results of simulation experiments,

$$P_{c,l,t} = sp_l + \sum_{i \in I} \sum_{l' \in L_i} DP_{c,l,t}^{(i,l')} + BP_{c,l,t} \Big|_{l=l1} \quad \forall c \in C, l \in L, t \in T \quad (13)$$

$$BP_{c,l,t} = \sum_{l \in L} \delta_l S_{c,l,t} \qquad \forall c \in C, t \in T \quad (14)$$

By combining all propagation mechanisms and directions, dynamic pressure is effectively mapped across the reservoir, as illustrated in Fig. 3.

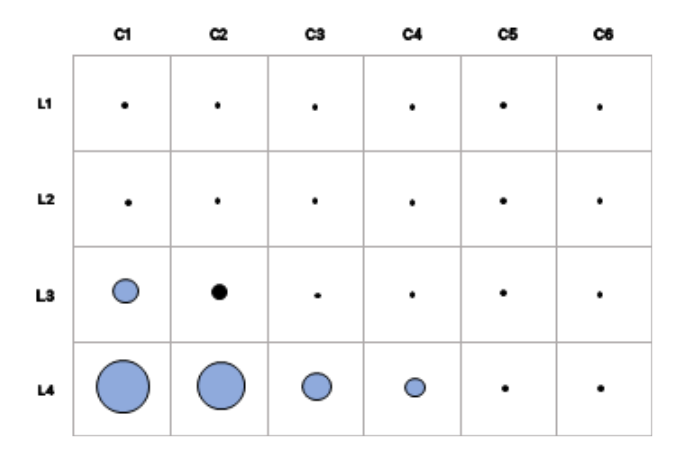


**Fig. 3.** Dynamic pressure propagation within the reservoir from injection at block (c1, l4). The size of the circles represents the magnitude of the pressure at each block.

## CO<sub>2</sub> material balance

An accurate characterization of CO<sub>2</sub> migration across the reservoir is essential to update the saturation map, which in turn allows the mathematical model to accurately represent the system's dynamic behavior according to pressure propagation. Additionally, the saturation of each block and the CO<sub>2</sub> flows toward the reservoir boundaries are key variables to ensure compliance with subsurface engineering policies during operation, as discussed later in this work. Given their importance, greater rigor in the calculation of these variables enables the adoption of less conservative injection strategies (which are very common in current industrial practice) ultimately maximizing the storage efficiency.

Firstly, it is necessary to track the amount of  $CO_2$  present in each block of the reservoir at every time period t. This is achieved using the mass balance equation presented in Eq. 15, which is given in volume units from the incompressibility assumption. In that equation,  $Q_{c,l,t}$  represents the total amount of  $CO_2$  (in volume units) contained into block (c, l) at time period t, and is defined as the sum of the  $CO_2$  present at the previous period plus the amount directly injected into that block from an injection point  $(QT_{l,c,l,t})$ , just for blocks adjacent to well injection points), also adding and subtracting the horizontal and vertical flows entering from and exiting to adjacent blocks  $(Q^H_{c-1,c,l,t}, Q^H_{c,c+1,l,t}, Q^V_{c,l+1,l,t})$  and  $Q^V_{c,l,l-1,t}$ , respectively). Note that  $Q^H_{c-1,c,l,t}, Q^H_{c,c+1,l,t}, Q^V_{c,l+1,l,t}$  and  $Q^V_{c,l,l-1,t}$  are unconstrained variables that may take negative values. More specifically, outgoing flows yield negative terms and are subtracted from the cumulative amount of  $CO_2$  stored in the block. In Eq. 15,  $\Delta t$  is the length of a time period, usually given in days.

$$Q_{c,l,t} = Q_{c,l,t-1} + \Delta t \left[ \sum_{i \in I} QT_{i,c,l,t} \Big|_{c,c+1 \in C_i} + Q_{c-1,c,l,t}^H - Q_{c,c+1,l,t}^H + Q_{c,l+1,l,t}^V - Q_{c,l,l-1,t}^V \right]$$
(15)
$$\forall c \in C, l \in L, t \in T$$

# CO<sub>2</sub> migration in the horizontal direction

Once again, Darcy's law is applied to predict  $CO_2$  migration in each direction; However, because every block is saturated with a two-phase fluid, yielding a heterogeneous medium, a new variable known as effective permeability must be incorporated into the analysis. As demonstrated in numerous studies, the effective permeability of a reservoir to a certain component of the multiphase fluid highly depends on its saturation (Ahmed, 2010). In our model, the effective permeability to  $CO_2$  is represented by means of a fourth degree polynomial function of the saturation, which accurately fits experimental data. The correlation adopted is presented in Eq. 16. The adjustment of the function to real data is illustrated in Fig. 4, where the factor  $\left(\frac{S_{c,l,t}}{S_{max}}\right)^4$  is usually referred to as the relative permeability,

$$KH_{c,l,t}^{eff} = kh_{c,l} \left(\frac{S_{c,l,t}}{S_{max}}\right)^4 \qquad \forall c \in C, l \in L, t \in T \quad (16)$$

Note that relative permeability, and consequently CO<sub>2</sub> movement, remains negligible until a certain threshold is reached. This threshold corresponds to approximately half of the maximum reachable saturation. This behavior is closely related to capillary effects, which lead to the so-called residual trapping. Since the reservoir is initially fully saturated with brine, a substantial amount of CO<sub>2</sub> is required to initiate fluid displacement farther than the receiving blocks. Residual trapping is a safe

storage mechanism that occurs as the CO<sub>2</sub> plume passes through porous rocks, leaving small amounts of CO<sub>2</sub> immobilized within the pore spaces. Under this mechanism, the carbon saturation in the pore space remains below the minimum threshold required to sustain mobility through an effective permeability to CO<sub>2</sub>, substantially higher than zero (see Fig. 4).

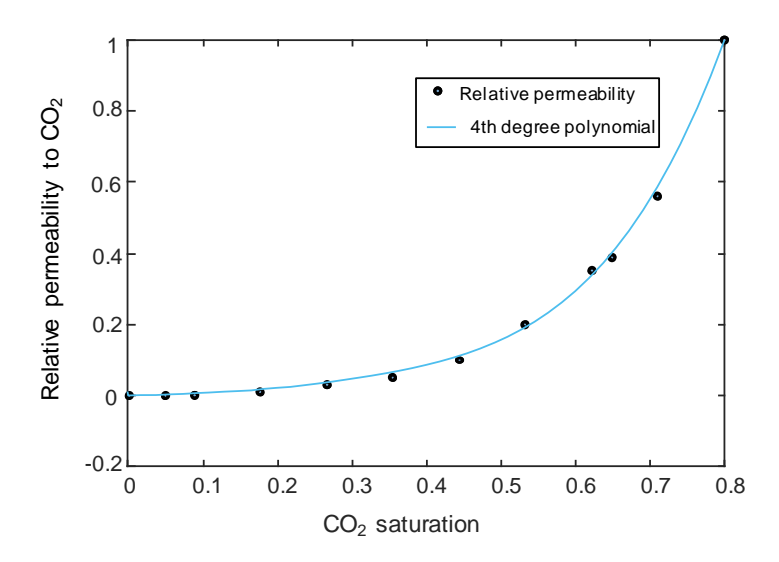


Fig. 4. Experimental data and polynomial correlation between relative permeability and saturation.

From the effective permeability in the horizontal direction  $(KH_{c,l,t}^{eff})$ , Darcy's law for heterogeneous flow is applied to predict  $CO_2$  migration to neighboring blocks in that direction. Such neighboring blocks share the same layer and correspond to contiguous columns as stated by Eq. 17. By convention, variable  $Q_{c,c',l,t}^H$  takes a positive value if  $CO_2$  migrates from c to c' = c + 1 and negative if it flows in the opposite direction. The flow direction will be determined by the difference of the pressures of adjacent blocks, which are driven by the propagation of dynamic pressures from the injection points of different wells.

$$Q_{c,c',l,t}^{H} = \frac{KH_{c,l,t}^{eff} \ area \left(P_{c,l,t} - P_{c',l,t}\right)}{\mu_{CO2} \ length}$$

$$\forall c \in C, c' = c + 1, l \in L, t \in T$$

## CO<sub>2</sub> migration in the vertical direction

Similarly, effective permeability to  $CO_2$  in the vertical direction is computed by Eq. 18 while Darcy's law is applied in Eq. 19 to predict  $CO_2$  migration along column c, from layer l to l-1 (upwards). By convention, variable  $Q_{c,l,l',t}^V$  takes a positive value if  $CO_2$  migrates from l to l'=l-1 and negative if it flows in the opposite direction. As stated by Eq. 19, the first driver for vertical migration is the

dynamic pressure gradient due to  $CO_2$  injection at different layers of different wells. Nevertheless,  $CO_2$  upwards movement is further driven by buoyancy forces, which are accounted for by the variable  $B_{c,l,l',t}$  in Eq. 19.

$$KV_{c,l,t}^{eff} = kv_{c,l} \left(\frac{S_{c,l,t}}{S_{max}}\right)^4 \qquad \forall c \in C, l \in L, t \in T \quad (18)$$

$$Q_{c,l,l',t}^{V} = \frac{KV_{c,l,t}^{eff} \ area \ \sum_{i \in I} \sum_{ll \in L_i} \left( DP_{c,l,t}^{(i,ll)} - DP_{c,l',t}^{(i,ll)} \right)}{\mu_{CO2} \ height} + B_{c,l,l',t}$$
(19)

$$\forall c \in C, l \in L, l' = l - 1, t \in T$$

The vertical flow rate due to buoyancy is driven by static pressure difference between sequential layers and is proportional to the difference of densities between  $CO_2$  and brine. Since buoyancy does not occur in a single slug, but is instead dispersed in bubbles (or small streamlines) across the entire cross-sectional area of a block, each  $CO_2$  bubble must overcome its own resistance. To account for this, the parameter  $\sigma \ll 1$  is introduced in Eq. 20, which can be adjusted to fit simulation data,

$$B_{c,l,l',t} = \frac{\rho_{brine} - \rho_{CO2}}{\rho_{brine}} (sp_l - sp_{l'}) \frac{kv_{c,l} \, \sigma \, S_{c,l,t-1} \, area}{\mu_{CO2} \, height}$$
(20)

$$\forall c \in C, l \in L, l' = l - 1, t \in T$$

Saturation of CO<sub>2</sub> at every block

Lastly, by knowing the void-volume of a block  $(avol_{c,l})$  computed as in Eq. 21 from its porosity  $\varphi_{c,l}$ , Eq. 22 calculates the CO<sub>2</sub> saturation  $S_{c,l,t}$  in each block (c, l) at time t. It should be noted that the effective volume available for storage may vary with the porosity  $\varphi_{c,l}$ . Since boundary blocks in columns  $c \in CB$  are assumed to have an infinite volume, saturation calculation is omitted for those blocks.

$$avol_{c,l} = \varphi_{c,l} \cdot length \cdot height \cdot width$$
  $\forall c \in C - CB, l \in L$  (21)

$$S_{c,l,t} = \frac{Q_{c,l,t}}{avol_{c,l}} \qquad \forall c \in C - CB, l \in L, t \in T \quad (22)$$

## **Subsurface operational constraints**

Besides the set of equations proposed to model reservoir dynamics, additional constraints must be included to ensure reservoir integrity and maintain safe operational conditions. Although subsurface policies have been addressed in previous works, they are rarely implemented as strict constraints to be satisfied during the optimization process. Instead, heuristic approaches often embed constraint violations within the objective function, and subsequently refine the solution to better comply with

them. With the development of a simplified yet accurate representation of reservoir fluid dynamics in both space and time domains, these policies can now be directly incorporated as constraints within the mathematical programming model, allowing for a more rigorous and integrated approach that can effectively address operational safety and reservoir integrity.

## Managing pressures

Managing the pressure build-up resulting from CO<sub>2</sub> injection is essential to prevent the occurrence of fracture phenomena (Nicot, 2008). To address this, a maximum admissible pressure is imposed for each block as defined in Eq. 23. This upper limit ensures operational safety and significantly influences CO<sub>2</sub> injection dynamics. As demonstrated by Szulczewski et al. (2011), restricting pressure build-up within the reservoir substantially impacts injection performance in the short term.

$$P_{c,l,t} \le p_{c,l}^{max} \qquad \forall c \in C, l \in L, t \in T \quad (23)$$

Moreover, the injectivity is also limited by the maximum admissible bottom-hole pressure (BHP) at each well as stated in Eq. 24. Maximum BHPs promote predictable and safe behavior, not only within the reservoir, but also in the operational equipment. Pressure constraints ensure that the injection process remains within design parameters, reducing the risk of equipment failure and maintaining the integrity of the storage system.

$$BHP_{i,t} \le bhp_i^{max} \quad \forall i \in I, t \in T \quad (24)$$

## Managing saturation

In contrast to pressure constraints, porosity and resulting effective storage capacity play a more significant role over the long term. Saturation level at each block is restricted by Eq. 25 to a given maximum, which is typically set at values around 0.80,

$$S_{c,l,t} \le s_{max}$$
  $\forall c \in C, l \in L, t \in T$  (25)

#### Plume extension

Recognizing that the primary trapping mechanisms are of residual and structural types (Raza et al., 2018), effective control at the grid boundaries is essential to ensure that the  $CO_2$  plume does not exceed the control volume limits. Eq. 26 imposes a small upper bound  $\varepsilon$  on the total amount of  $CO_2$  that can move horizontally into the boundary cells over the long-term planning horizon. This is typically defined by the relevant regulatory authority to threshold values close to zero.

$$\sum_{c \in CB, l \in L} Q_{c, l, T} \le \varepsilon \tag{26}$$

Note that during and even after injection, buoyancy forces continue to promote upward displacement of CO<sub>2</sub>, which limits the horizontal spread of the CO<sub>2</sub> plume in deep layers, reducing its access to fresh brine within the aquifer (Ismail & Gaganis, 2023). However, buoyancy provokes CO<sub>2</sub> spread when reaching the top layer (caprock), which can compromise containment in the very long term. All these aspects introduce a difficult trade-off to be solved while searching for the optimal injection policy. The strategy must balance the safety of the trapping mechanisms against maximizing the effective utilization of the storage volume over the time horizon.

## CO<sub>2</sub> availability

Lastly, certain limitations on the  $CO_2$  injection policy arise from capacity constraints in upstream operations. One such limitation is  $CO_2$  availability, as carbon must first be captured, prior to injection. This model does not optimize over upstream carbon capture processes, but instead assumes a predefined parameter  $co2_t^{max}$  that represents the maximum amount of  $CO_2$  available for injection across the reservoir during each time period. Accordingly, an upper bound is imposed on the total injection of  $CO_2$  over all wells for every period t, as stated by Eq. 27,

$$\sum_{i \in I} Y_{i,t} \le co2_t^{max} \qquad \forall t \in T \quad (27)$$

In practice, the time horizon is divided into injection and passive phases. While balance equations and migration constraints need to be tracked all along the time horizon, massive injection is only allowed over the injection phase (first TI periods). Therefore,  $CO_2$  availability given by parameter  $co2_t^{max}$  is reduced to a relatively small value for later periods t > TI, with the only purpose of maintaining the reservoir stability.

An important aspect to emphasize is that despite the large number of equations and variables required to capture the complexity of the problem (in the order of thousands for a relatively small case), each variable can ultimately be expressed as a function of the bottom-hole pressures in every well i up to period t ( $BHP_{i,t'}$ ,  $t' \le t$ ), making them the only true decision variables. Consequently, the problem has relatively few degrees of freedom to manipulate in the search for the optimal solution. This characteristic enhances the performance of reduced-gradient solvers, even when dealing with a highly nonlinear model. However, it may also yield suboptimal solutions, such as the zero-injection scenario, due to the limited flexibility in the decision space. Ongoing research is focused on developing more robust approaches that improve convergence and can guarantee global optimal solutions.

## **Objective function**

An optimal injection strategy must carefully manage pressure increases and CO<sub>2</sub> containment throughout the reservoir. This may involve strategically manipulating injection rates at different wells to enhance pressure propagation toward the reservoir boundaries, thereby maximizing storage efficiency while ensuring safe operations. Since safe storage conditions have been addressed through the constraints previously discussed, the primary focus of the objective function, defined in Eq. 28, is simply to maximize the total amount of CO<sub>2</sub> injected into the reservoir over the time horizon,

$$Max z = \sum_{i \in I} \sum_{t \in T} Y_{i,t}$$
 (28)

In summary, the NLP formulation aims to maximize Eq. 28 subject to the reservoir dynamics equations (Eqs. 2-22) and subsurface engineering policies (Eqs. 23-27) that ensure safe operations.

## Results and discussion

This section presents several instances of different case studies aimed at optimizing the CO<sub>2</sub> injection plan for illustrative, two-dimensional reservoirs. The optimization results are obtained from the NLP model developed in the previous section, whose goal is to maximize CO<sub>2</sub> storage efficiency while adhering to operational and regulatory constraints. The mathematical model is implemented using GAMS 45.3.0 (GAMS, 2023), and all NLP optimization runs are solved with CONOPT4, the latest version of CONOPT (Drud, 1996). Computations are performed on a system with an Intel Core i7 13<sup>th</sup> Gen CPU (1.7 GHz, 16 GB RAM), utilizing up to 12 threads for parallel processing. Note that nonlinear equations can be expressed in quadratic terms, yielding a nonconvex QCP formulation. However, for all the cases presented in this work, specific QCP global solvers like GUROBI cannot find even a good feasible solution after hours of computation.

For illustrative purposes, the optimization model considers a 20-year horizon, discretized into annual time periods, during which two vertical injection wells are operated. For the first 10 years, the CO<sub>2</sub> injection rate into each well is considered as a decision variable, subject to an upper limit of 0.5 Mton per year. This injection capacity corresponds to the annual CO<sub>2</sub> emissions of a small 100 MW coal-fired power plant. Based on this fact, the selected rate is deemed appropriate, given that the reservoir model provides a conservative estimation of the storage capacity by not fully accounting for its three-dimensional nature. If the total available CO<sub>2</sub> is injected, it would occupy approximately 2% of the reservoir's pore volume, which falls within the 1–4% range suggested by the Intergovernmental Panel on Climate Change (Solomon, 2007).

During the injection phase, the primary constraints influencing the optimization procedure are injectivity limitations and pressure build-up restrictions. To ensure operational safety, the bottom-

hole pressure is constrained to a maximum of 30 MPa, which corresponds to approximately 1.5 times the initial reservoir pressure. Additionally, the pressure in each grid block is limited to 35 MPa to prevent potential reservoir fracturing or leakage.

After the injection phase, the model is also intended to keep track of the CO<sub>2</sub> plume extension over the following 10 years. The optimization framework enforces containment constraints over the whole time horizon, ensuring that the migration of CO<sub>2</sub> remains within the designated storage area. Specifically, the model imposes a maximum threshold of 0.0015 Mton at the reservoir boundaries, thereby mitigating the risk of unintended plume expansion beyond regulatory limits.

The rest of the section is structured as follows. First, we present a detailed description of an illustrative reservoir with homogenous properties, including the necessary assumptions for its implementation. Next, we analyze the results from an initial set of scenarios (*Case 1*), which involve simplified well placement designs and reservoir representations. These preliminary scenarios primarily serve to visualize the fundamental principles governing the model, and to conduct a basic sensitivity analysis on the influence of injection rates and well depths. Following this, we extend our analysis using a higher-fidelity model (*Case 2*), incorporating finer grid spatial resolution to improve the accuracy of the results and validate the injection strategies. Finally, we apply the model to a reservoir featuring a realistic permeability field (*Case 3*), allowing for a more comprehensive assessment of the relationship between the reservoir's geophysical characteristics and the optimization strategy that maximizes CO<sub>2</sub> storage.

### **Reservoir representation**

The illustrative reservoir is located 1200 meters below the surface, and extends over 4800 x 100 x 700 meters. Assuming a fixed, homogeneous porosity of 0.12, the total pore volume is estimated at 40.32 million cubic meters.

A grid block aspect ratio of 2:1:1 (length: thickness: height) is adopted. For *Case 1* and *Case 3* the model employs a spatial discretization of 24 x 1 x 7 grid blocks (see Fig. 5). In *Case 2*, a higher fidelity model is introduced, refining the spatial resolution to 48 x 1 x 14. In *Case 1* and *Case 2*, a homogeneous permeability of 250 mD is assumed all across the field, with vertical permeability set as 1% of the horizontal permeability. Subsequently, in *Case 3*, a synthetic heterogeneous permeability field is introduced to resemble realistic reservoir conditions, allowing for a more accurate evaluation of the CO<sub>2</sub> injection strategy.

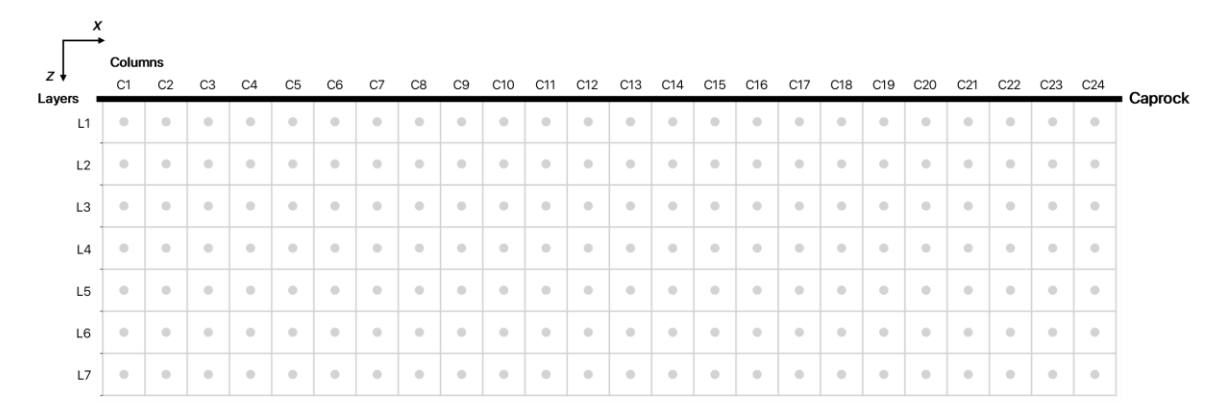


Fig. 5. Two-dimensional grid discretization for the optimization model.

## Case study 1

## Instance 1.1: Deep wells

This case emulates a criterion for injection planning that guides common industry practices. Based on comments from our industry partner, well operators might favor deeper injection wells to slow down buoyancy forces. In shallow wells, buoyancy drives CO<sub>2</sub> upward, increasing the risk of early structural trapping and CO<sub>2</sub> dispersion. Besides, during its ascent, CO<sub>2</sub> interacts with brine, enhancing dissolution and residual trapping, which provide safer long-term storage. Therefore, prolonging the vertical migration path until reaching the caprock can be one of the key objectives. On the other hand, a balanced injection strategy is also standard practice, particularly in early-stage operations when reservoir behavior is uncertain. Reducing variability in injection rates across wells simplifies CO<sub>2</sub> migration forecasts, improving operational control. Based on practical considerations, *Case 1* comprises two wells that are placed in the second-lowest reservoir layer (*L6*). Note that layer *L7* is kept within the model to track vertical migration, but is not used for injection to avoid boundary effects. The first injection well (*IW1*) is positioned between columns *C8* and *C9*, while *IW2* is located between *C16* and *C17*. Additional constraints are included in the optimization model to ensure an even distribution of injection rates among the wells over time.

The NLP model of *Case 1.1* comprises 73,141 constraints and 71,161 variables, with 43,274 nonlinear elements in the Jacobian matrix. Despite its large scale, the degrees of freedom remain limited to bottom-hole pressures per well at each time step, from which injection rates are derived. Over the first 10 years, the total amount of CO<sub>2</sub> injected reaches 0.14 Mton, storing merely 3% of the available CO<sub>2</sub>. As demonstrated later in this section, this amount can increase significantly. One of the primary reasons why the initial well placement strategy fails to maximize reservoir storage capacity, despite following the general guideline of "the deeper, the better", is the pressure interference between the

wells. Since both wells inject simultaneously at similar rates, dynamic pressure buildup in the central region limits injectivity to remain within regulatory pressure constraints, and forces CO<sub>2</sub> flows to move toward the reservoir boundaries. As a result, the central section between the wells remains mostly underutilized, preventing fresh brine from interacting with newly injected CO<sub>2</sub>, thereby hindering the activation of safe trapping.

### *Instance 1.2: Layer shifting*

To evaluate a different design that can avoid pressure interference, the well placement strategy is modified in *Case 1.2* by relocating *IW2* to a different injection layer. Since pressure propagation predominantly occurs in the horizontal direction shifting *IW2* to *L4*, while maintaining its original column position reduces direct pressure overlap (see Fig. 6 for well placement illustration).

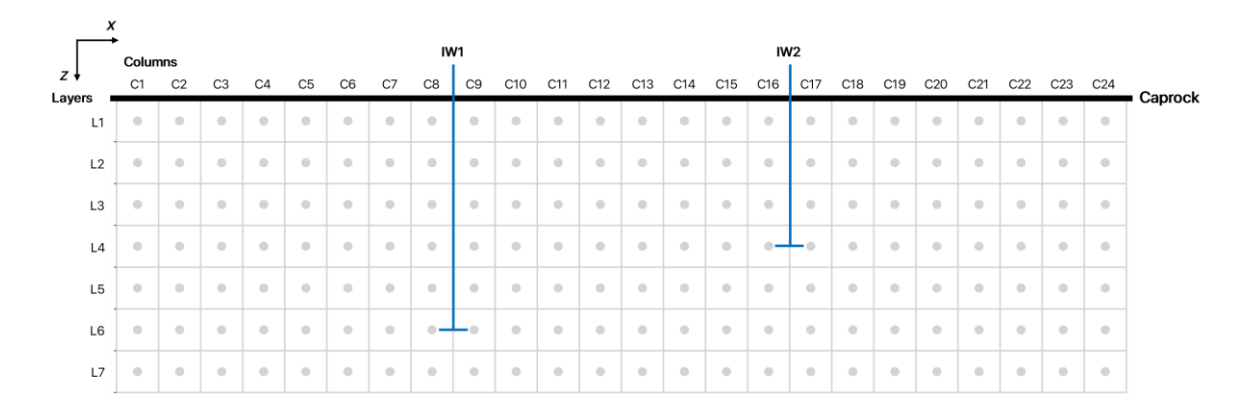


Fig. 6. Well layout for Case 1.2.

After solving the NLP model proposed in this work, the revised design shows a significant improvement in the storage efficiency. The optimization model now achieves a total injection of 1.25 Mton of CO<sub>2</sub>, representing an eight-times increase compared to the initial design. More than 25% of the total available CO<sub>2</sub> can be injected under these conditions. The results confirm that shifting injection depths can enhance storage efficiency by minimizing pressure interference. Another key observation from these results is that the primary limiting factor is not CO<sub>2</sub> plume extension, but rather injectivity constraints. One indicator supporting this conclusion is the dominance of vertical migration over horizontal spread. As previously discussed, when injection pressure is sufficiently high, the CO<sub>2</sub> plume yields a flatter front, allowing viscous forces to overcome buoyancy and extend further into the reservoir. However, due to the imposition of equivalent injection rates at both wells, the system can never reach the threshold where viscous forces dominate over gravity-driven migration. At this point, it becomes evident that injection strategies can greatly benefit from managing different injection rates per well.

## Instance 1.3: Decoupling injection rates

Building upon the previous design, we conduct a final experiment (*Case 1.3*) in which the constraint of balanced injection rates is lifted, favoring unrestricted optimization of injection rates per well. By introducing this flexibility, the total CO<sub>2</sub> injection increases further to 2.23 Mton, representing nearly 45% of the available carbon. Note that the improvement in the objective function stems from the implementation of alternating injection strategies as illustrated on Fig. 7. As shown by previous authors (Zou and Durlofsky, 2023), alternating strategies can mitigate pressure interference leading to high injection rates at specific periods to promote a more uniform CO<sub>2</sub> plume front, also enhancing residual trapping. In real-world scenarios, this strategy would also favor dissolution trapping, which was not explicitly considered in this version of the model. The results also reveal that alternate injection allows CO<sub>2</sub> to redistribute, reducing pressure build-up and preventing local saturation from reaching its upper limit.

A key observation from this case is that the primary limiting constraint has now shifted from injectivity to plume containment, as CO<sub>2</sub> reaches the maximum regulatory threshold at the reservoir boundaries. Fig. 8 illustrates CO<sub>2</sub> saturation maps at two critical time points: the end of the injection phase (Year 10), and the end of the time horizon (Year 20). To provide better visualization, an upscaled, smoother version of the saturation map is also shown in the same figure. As expected, once injection ceases, dynamic pressure no longer dictates carbon movement, leaving vertical migration due to gravity as the predominant transport mechanism.

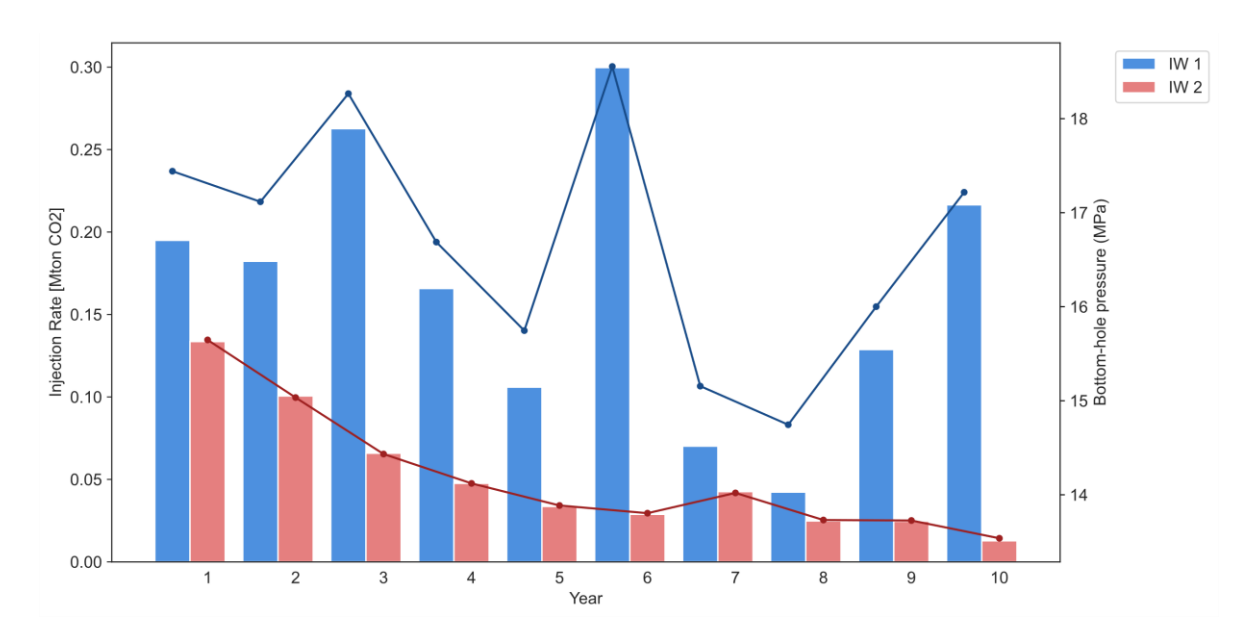


Fig. 7. Case 1.3 optimized CO<sub>2</sub> injection profiles (bars) and bottom-hole pressure (lines) for each well over injection horizon.

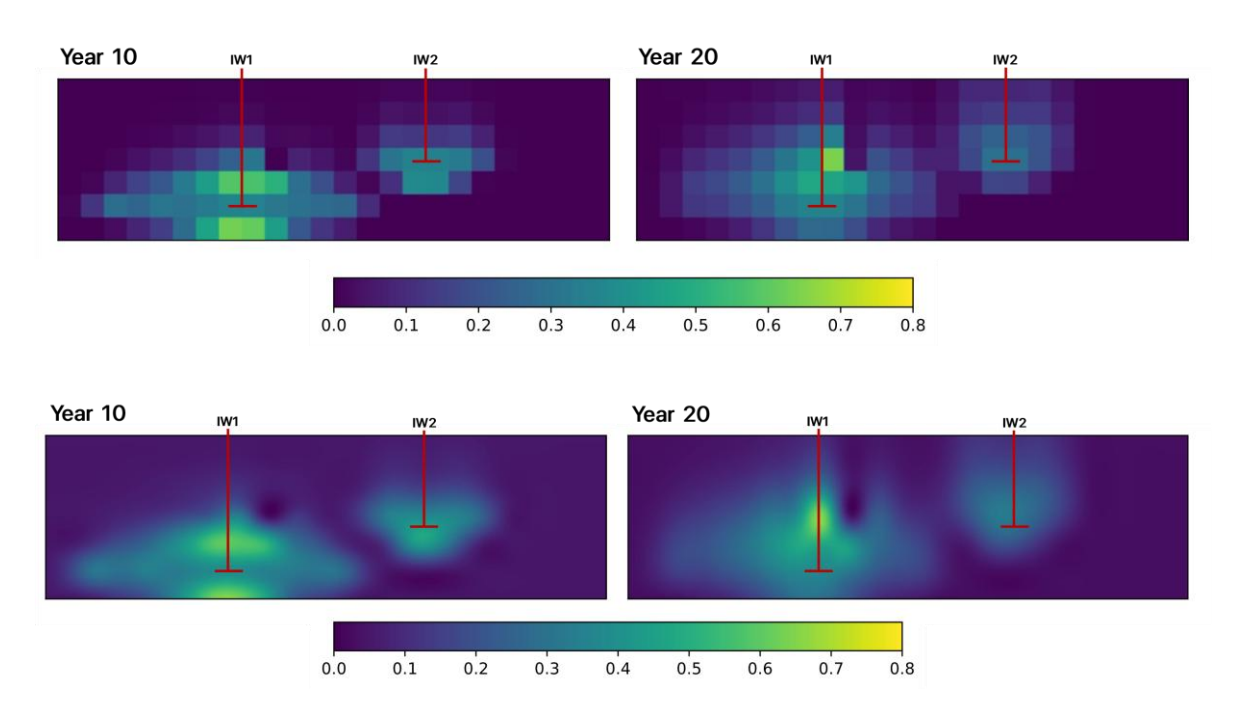


Fig. 8. Resulting saturation map for Case 1.3 at the end of injection phase (left) and end of control horizon (right).

Table 1. Model parameters and results for all case studies and instances

	Case 1.1	Case 1.2	Case 1.3	Case 2	Case 3
Grid discretization	24 x 1 x 7	24 x 1 x 7	24 x 1 x 7	48 x 1 x 14	24 x 1 x 7
Injection layers	IW1.L6; IW2.L6	IW1.L6; IW2.L4	IW1.L6; IW2.L4	IW1.L6; IW2.L4	IW1.L6; IW2.L4
Horizontal permeability	Constant 250 mD	Constant 250 mD	Constant 250 mD	Constant 250 mD	Log-normally distributed (420; 100) mD
Vertical permeability $k_{ m v}/k_{ m h}$	0.01	0.01	0.01	0.01	0.01
Constraints on injection profile	Balanced injection	Balanced injection	None	None	None
Model size	73,061 const; 71,161 vars.	73,061 const; 71,161 vars.	73,061 const; 71,161 vars.	422,061 const; 413,761 vars.	73,061 const; 71,161 vars.
CPU Time [s]	12.27	23.28	111	2075	209
Objective value [Mton CO <sub>2</sub> ]	0.14	1.25	2.23	1.76	2.45

The resulting injection plan for *Case 1.3* has been validated using commercial simulation software (GEM, by Computer Modelling Group Ltd.) broadly used in the CCS industry. Using different grid resolutions, results from the NRS favorably compare with predictions made by the optimization model. Results and statistics from simulation are provided in the Supplementary Material.

Computational details for all instances of *Case study 1* are presented in Table 1, while the full set of results from the optimal solutions are presented in the Supplementary Material. Note that in all instances of *Case 1* the optimal solutions are obtained in less than two minutes of CPU time.

### Case study 2

The aquifer model used in *Case 1* has been intentionally designed with a relatively coarse grid to ensure computational efficiency. To assess the impact of grid resolution on model sizes, CPU times and optimal solutions, we now address the CO<sub>2</sub> injection planning under the same conditions of *Case 1.3* but using a refined spatial discretization of 48 x 1 x 14, yielding a total of 672 grid blocks. This refinement significantly increases model dimensions, expanding to 422,061 constraints and 413,761 variables, i.e. a fivefold increase after dividing the blocks in quarters.

In the optimal solution, the total amount of CO<sub>2</sub> that can be sequestered at the end of the injection phase is 1.76 Mton, which is 20% smaller than the injection volume obtained using the coarse-grid model. This outcome aligns with prior research findings, which indicate that coarse-grid representations tend to underestimate plume migration, leading to an overestimation of storage efficiency (Yamamoto et al., 2011; Zou and Durlofsky, 2023). The computational performance of the NLP model is promising since even for a finer discretization, the solver finds the local optimal solution in less than 35 minutes of CPU, as shown in Table 1. Details on the solution for *Case 2* are presented in the Supplementary Material.

## Case study 3

For the first two cases we have assumed a homogeneous aquifer, which does not represent real-world reservoir features accurately. In practice, geophysical properties vary spatially, influencing CO<sub>2</sub> injection and migration dynamics. As a result, well injection performance is strongly dependent on local reservoir characteristics, requiring smarter injection strategies that can adapt to heterogeneities. Field engineers typically obtain subsurface data at discrete locations, and various interpolation and simulation techniques allow for constructing data-driven geophysical realizations of the field. One

widely applied method is Sequential Gaussian Simulation (SGS), which is used in this work to generate a synthetic permeability map as shown in Fig. 9.

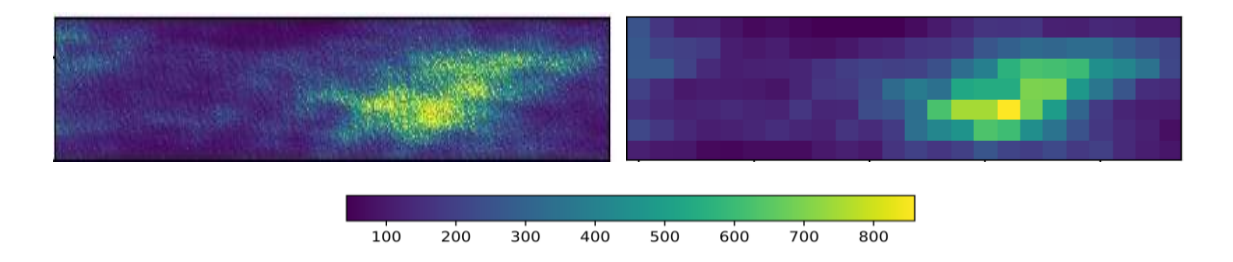


Fig. 9. 480 x 70 synthetic permeability field for Case 3 (left) and its aggregated 24 x 7 representation (right).

More specifically, the heterogeneous permeability field is generated using the built-in function gs.SRF of the GSTools geostatistical Python framework (Müller et al., 2022). A spherical variogram model is applied to a 480 x 70 two-dimensional grid, with correlation lengths of  $l_x/L_x=0.6$  and  $l_z/L_z=1$  in the horizontal and vertical directions, respectively. Permeability follows a log-normal distribution, with log- permeability mean of 420 and standard deviation of 100. The  $k_v/k_h$  ratio remains fixed at 0.01, consistent with previous cases.

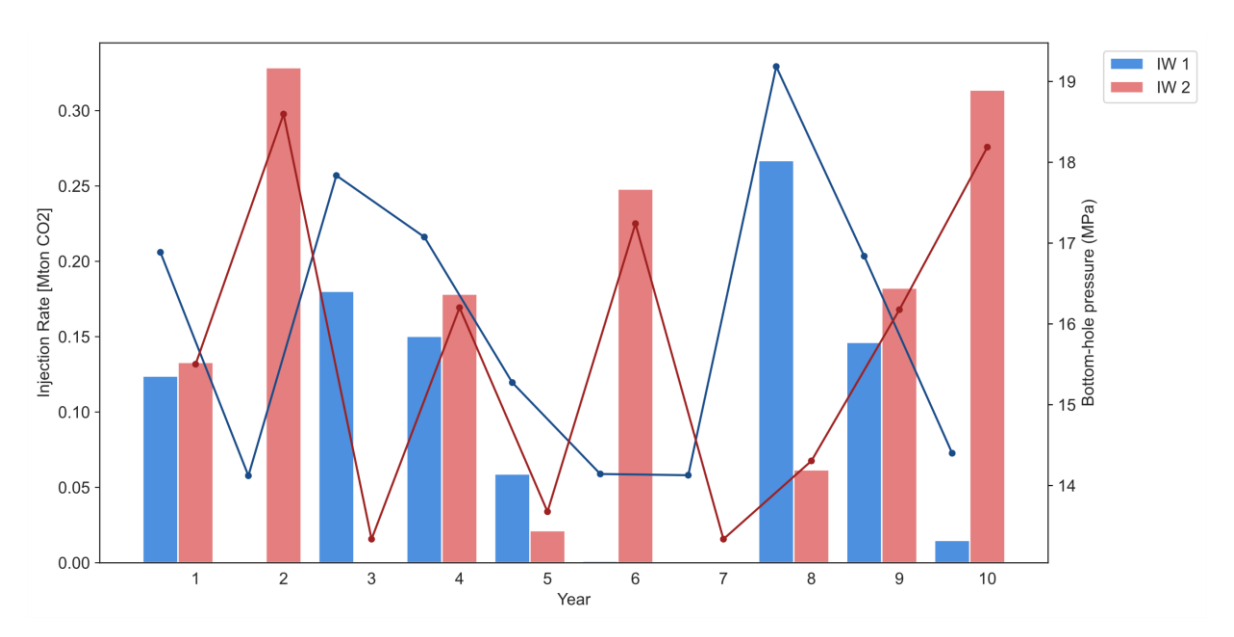


Fig. 10. Optimized CO<sub>2</sub> injection profiles (bars) and bottom-hole pressure (lines) for each well in Case study 3.

In short, the injection plan of *Case study 3* is optimized under similar conditions as in *Case 1.3*, but now based on the heterogeneous permeability field depicted at the right of Fig. 9. The optimal solution from the NLP proposed in this work yields a total CO<sub>2</sub> storage of 2.45 Mton, which is obtained after 209 s of CPU time (see Table 1). Fig. 10 presents the injection strategy and bottom-

hole pressure profile for each well during the injection phase. Remarkably, the injection is preferentially distributed (60-40%) toward *IW2*, which is shallower but located in a higher-permeability zone, capped by low-permeability blocks at layer *L1*. An important observation is that the interference of dynamic pressures from the two wells is more important than in *Case 2*, despite the shift in depth. This occurs due to the presence of higher permeability paths between the injection points. As a result, identifying the optimal solution becomes more complex, and cannot be easily determined through manual adjustment or direct search methods. This highlights the advantage of using an advanced optimization model to efficiently navigate problem complexities.

Another noteworthy point is that each well operates under a distinct active constraint. *IW2* is limited by plume migration because high permeability accelerates CO<sub>2</sub> movement toward the top-right boundary of the aquifer (see Fig. 11). In contrast, *IW1* is constrained by pressure buildup, requiring longer pausing periods to allow the plume to redistribute and facilitate additional CO<sub>2</sub> injection in the surrounding region. These findings reinforce that the dominant constraint (or set of constraints) varies spatially, directly shaping the optimal injection strategy into heterogeneous reservoirs.

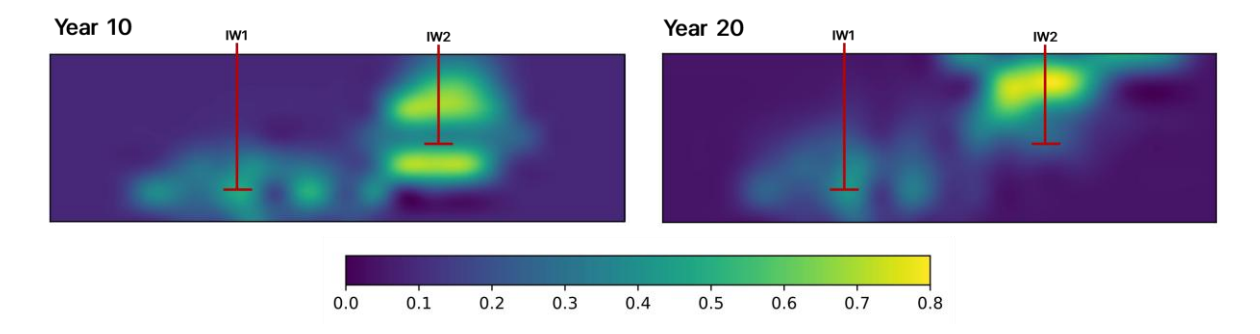


Fig. 11. Resulting saturation map for Case 3 at the end of injection phase (left) and end of control horizon (right).

One key aspect that is left for future work is the adjustment of the parameters of the optimization model in order to accurately predict plume migration and pressure gradients, even when using coarse grids. This could be done in sequential steps, by comparing with the results of simulation runs based on much finer discretizations.

## **Conclusions**

We have proposed an efficient mathematical programming model to optimize the storage of CO<sub>2</sub> into deep saline aquifers in the long term. The NLP optimization model relies on well-known physics models like Darcy's law that allow to capture migration of CO<sub>2</sub> based on permeability, saturation and pressure gradients. The NLP formulation is based on a time and volume discrete representation that

has been initially deployed in two dimensions, using finite-difference algebraic equations. The computational results are quite promising since they suggest that the model may scale reasonably to real instances and 3D configurations. For the optimization model to be practical, it must maintain fast computational runtime, otherwise it offers little advantage over the metaheuristic methods discussed in this paper, which rely on sequential, computationally expensive function evaluations via numerical reservoir simulation. In fact, we have not sought to replicate the accuracy of NRS, but rather to guide the development of injection strategies that can also enable field operators to rapidly explore different well designs. While higher-fidelity models remain essential for final validation, our approach avoids the need to evaluate hundreds or even thousands of candidate solutions as required by previous approaches. Instead, only the optimal solution yielded by the mathematical model will be tested, adjusted and eventually validated, thus reducing the overall computational cost significantly.

It is interesting to note that the results shown in this paper have been found using CONOPT4, a generalized reduced-gradient local solver (Drud, 1996). It is not surprising to see that this active set, feasible path solver yields very good results for an NLP model with thousands of equality constraints and just a few bounds. Following a feasible path, it computes relevant derivatives, and therefore better directions towards the optimal solution. The feasibility of the initial and intermediate points, satisfying thousands of complex material and pressure balances is expensive, and thus, carefully preserved by the solution strategy. Although the NLP model can be fully expressed in quadratic terms, specific global solvers for QCP like GUROBI struggle to find even a good feasible solution in reasonable CPU times.

Further experimentation, model adaptations to account for solubility trapping, and extensions to 3D are ongoing work. The development of an iterative, self-adaptive optimization framework capable of solving real-world instances in reasonable times is the final goal of this project.

# Acknowledgments

Financial support from National University of Litoral under Grant CAI+D 2020, from ANPCyT under Grant PICT 2020-1783 and from CONICET under Grant PIP 2021 is gratefully acknowledged. Financial support from Air Products and Chemicals, Inc. through the Center for Advanced Process Decision-making at Carnegie Mellon University is also gratefully acknowledged.

## **Nomenclature**

Sets and subscripts

 $c \in C$  columns (grid discretization in the x-direction)

 $c \in C_i$  column at the right of well i

 $c \in CB$  columns located at the boundaries of the grid

 $i \in I$  injection wells

 $l \in L$  layers (grid discretization in the z-direction)

 $l \in L_i$  layers into which well i injects CO<sub>2</sub>

 $t \in T$  time periods

## Parameters [units]

area cross sectional area of a block [m<sup>2</sup>]  $avol_{c,l}$  effective volume of cell (c, l) [m<sup>3</sup>]

 $bhp_i^{max}$  maximum permissible bottom-hole pressure for each well i [MPa]

 $co2_t^{max}$  available CO<sub>2</sub> for injection in time period t [m<sup>3</sup>/s]

 $depth_o$  depth at top of the reservoir [m]

 $depth_l$  depth at layer l [m]

g gravitational acceleration [m/s<sup>2</sup>]

height height of a grid block [m]

 $kh_{c,l}$  reservoir horizontal permeability of block (c, l) [mD]  $kv_{c,l}$  reservoir vertical permeability of block (c, l) [mD]

length length of a grid block [m]

 $n_{diss}$  number of blocks along which dynamic pressure is assumed to fully dissipate

 $p_{c,l}^{max}$  maximum permissible pressure for each block [MPa]

 $s_{max}$  maximum permissible CO<sub>2</sub> saturation for each block [-]

 $sp_l$  hydrostatic pressure in layer l [MPa]

width width of a grid block [m]

lpha horizontal flowrate fraction after vertical diversion [-]  $\delta_l$  weight for layer l to compute buoyancy pressure [MPa]

 $\Delta t$  length of a time period [days]

 $\varepsilon$  maximum amount of CO<sub>2</sub> allowed to reach boundaries [m<sup>3</sup>]

 $\varphi_{c,l}$  porosity of block (c, l) [-]  $\mu_{brine}$  viscosity of brine [ $\mu$ Pa s]

$\mu_{CO_2}$	viscosity of CO <sub>2</sub> [µPa s]				
$ ho_{CO_2}$	density of CO <sub>2</sub> [kg/m <sup>3</sup> ]				
$ ho_{brine}$	density of brine [kg/m³]				
σ	sparsity parameter for flow driven by buoyancy [-]				
Variables [units]					
$B_{c,l,l-1,t}$	vertical flow of CO <sub>2</sub> driven by buoyancy from block $(c, l)$ to $(c, l-1)$ at time $t$ [m³/day]				
$BHP_{i,t}$	bottom-hole pressure (measured at the top of the grid) of well $i$ at time period $t$ [MPa]				
$BP_{c,l,t}$	buoyancy pressure into the column $c$ of the top layer, at time period $t$ [MPa]				
$DP_{c,l,t}^{(i,l')}$	dynamic pressure at block $(c, l)$ originated from injection into well $i$ , layer $l$ , at time period $t$ [MPa]				
$KH_{c,l,t}^{eff}$	effective horizontal permeability for $CO_2$ in block $(c, l)$ at time period $t$ [mD]				
$KV_{c,l,t}^{eff}$	effective vertical permeability for $CO_2$ in block $(c, l)$ at time period $t$ [mD]				
$P_{c,l,t}$	pressure of block $(c, l)$ at time period $t$ [MPa]				
$Q_{c,l,t}$	amount of $CO_2$ in block $(c, l)$ at time period $t$ [m <sup>3</sup> ]				
$QT_{i,c,l,t}$	flow of $CO_2$ injected into block $(c, l)$ from well $i$ during time period $t$ [m³/day]				
$Q_{c,c+1,l,t}^H$	horizontal flow of $CO_2$ from block $(c, l)$ to block $(c+1, l)$ during time period $t$ [m³/day]				
$Q_{c,l,l-1,t}^V$	vertical flow of CO <sub>2</sub> from block $(c, l)$ to block $(c, l-1)$ during time period $t$ [m <sup>3</sup> /day]				
$S_{c,l,t}$	saturation of block $(c, l)$ at time period $t$ [-]				
$Y_{i,t}$	total amount of $CO_2$ injected into well $i$ at time period $t$ [m <sup>3</sup> ]				
Z	total amount of CO <sub>2</sub> injected in reservoir over the time horizon [m³]				
$\mu avg_{c,l,t}$	average viscosity at block $(c, l)$ during time period $t  [\mu Pa  s]$				

# References

- [1] Abadie, J., Carpentier J., 1969. Generalization of the Wolfe reduced gradient method to the case of nonlinear constraints in Optimization, R. Fletcher, Ed., Academic Press, 37-47.
- [2] Abhijnan A., Desai K., Wang J., Rodríguez-Martínez A., Dkhili N., Jellema R., Grossmann I.E., 2024. Mixed-Integer Nonlinear Programming Model for Optimal Field Management for Carbon Capture and Storage. Ind. Eng. Chem. Res., 63; 12053–12063.
- [3] Ahmed, T., 2010. Chapter 5 Relative Permeability Concepts. In: Ahmed, T. (Ed.), Reservoir Engineering Handbook (Fourth Edition). Gulf Professional Publishing, pp. 288–330. ISBN: 9781856178037. https://doi.org/10.1016/B978-1-85617-803-7.50013-4.
- [4] Air Products and Chemicals Inc., 2025. Louisiana Clean Energy Complex. https://www.airproducts.com/energy-transition/louisiana-clean-energy-complex (accessed 19 March 2025).

- [5] Biegler, L.T, 2010. Nonlinear Programming: Concepts, Algorithms, and Applications to Chemical Processes. SIAM Pub. Lib. ISBN: 9780898719383
- [6] Birkholzer, J.T., Oldenburg, C.M., Zhou, Q., 2015. CO2 migration and pressure evolution in deep saline aquifers. Int. J. Greenh. Gas Control 40, 203–220.
- [7] Borda, E.S., Govindan, R., Elahi, N., Korre, A., Durucan, S., 2017. The development of a dynamic CO2 injection strategy for the depleted Forties and Nelson oilfields using regression-based multi-objective programming. Energy Procedia 114, 3335–3342.
- [8] Cameron, D.A., Durlofsky, L.J., 2012. Optimization of well placement, CO2 injection rates, and brine cycling for geological carbon sequestration. Int. J. Greenh. Gas Control 10, 100–112.
- [9] Celia, M.A., Bachu, S., Nordbotten, J.M., Bandilla, K.W., 2015. Status of CO2 storage in deep saline aquifers with emphasis on modeling approaches and practical simulations. Water Resour. Res. 51, 6846–6892.
- [10] Darcy, H., 1856. Les fontaines publiques de la ville de Dijon. Paris: Dalmont.
- [11] Doughty, C., 2013. User's Guide for Hysteretic Capillary Pressure and Relative Permeability Functions in TOUGH2, Report LBNL-6533E, Lawrence Berkeley National Lab., Berkeley, CA.
- [12] Drud, A.S., 1996. CONOPT—a large-scale GRG code. ORSA J. Comput. 6 (2), 207–216.
- [13] GAMS Development Corporation, 2023. General Algebraic Modeling System (GAMS) Release 45.3.0. Fairfax, VA, USA.
- [14] Hasan, M.M.F., Zantye, M.S., Kazi, M.K., 2022. Challenges and opportunities in carbon capture, utilization and storage: A process systems engineering perspective. Comput Chem Eng. 166: 107925. https://doi.org/10.1016/j.compchemeng.2022.107925.
- [15] Hooke, R., Jeeves, T.A., 1961. "Direct Search" solution of numerical and statistical problems. J. ACM 8 (2), 212–229.
- [16] Ismail, I., Gaganis, V., 2023. Carbon capture, utilization, and storage in saline aquifers: Subsurface policies, development plans, well control strategies and optimization approaches—A review. Clean Technol. 5 (2), 609–637.
- [17] Kennedy, J., Eberhart, R., 1995. Particle swarm optimization. Proc. ICNN'95 Int. Conf. Neural Networks, 1942–1948.
- [18] Kolda, T.G., Lewis, R.M., Torczon, V., 2003. Optimization by direct search: New perspectives on some classical and modern methods. SIAM Rev. 45 (3), 385–482.
- [19] Kumar, D., 2007. Optimization of well settings to maximize residually trapped CO<sub>2</sub> in geologic carbon sequestration. Master's Thesis, Stanford University, Stanford, CA.
- [20] Massarweh, O., Abushaikha, A.S., 2024. CO2 sequestration in subsurface geological formations: A review of trapping mechanisms and monitoring techniques. Earth-Sci. Rev., 104793.
- [21] Miller, D.C., Syamlal, M., Mebane, D.S., Storlie, C., Bhattacharyya, D., Sahinidis, N.V., et al., 2014. Carbon capture simulation initiative: A case study in multiscale modeling and new challenges. *Annu. Rev. Chem. Biomol. Eng.*, 5 (1), 301–323. https://doi.org/10.1146/annurev-chembioeng-060713-040249.
- [22] Müller, S., Schüler, L., Zech, A., Heße, F., 2022. GSTools v1.3: a toolbox for geostatistical modelling in Python. Geosci. Model Dev., 15, 3161–3182. <a href="https://doi.org/10.5194/gmd-15-3161-2022">https://doi.org/10.5194/gmd-15-3161-2022</a>.
- [23] Nicot, J.P., 2008. Evaluation of large-scale CO2 storage on fresh-water sections of aquifers: An example from the Texas Gulf Coast Basin. Int. J. Greenh. Gas Control 2, 582–593.
- [24] Ng, C.S.W., Amar, M.N., Ghahfarokhi, A.J., Imsland, L.S., 2023. A survey on the application of machine learning and metaheuristic algorithms for intelligent proxy modeling in reservoir simulation. Comput. Chem. Eng. 170, 108107.

- [25] Nocedal, J., Wright, S.J., 2006. Numerical Optimization, Second Ed., Series in Operations Research and Financial Engineering. Springer, New York.
- [26] Nordbotten, J.M., Celia, M.A., Bachu, S., 2005. Injection and storage of CO2 in deep saline aquifers: Analytical solution for CO2 plume evolution during injection. Transp. Porous Media 58, 339–360.
- [27] Pires, J., Martins, F., Alvim-Ferraz, M., Simões, M., 2011. Recent developments on carbon capture and storage: An overview. Chem. Eng. Res. Des., 89 (9), 1446–1460. https://doi.org/10.1016/j.cherd.2011.01.028.
- [28] Raza, A., Gholami, R., Rezaee, R., Bing, C.H., Nagarajan, R., Hamid, M.A., 2018. CO2 storage in depleted gas reservoirs: A study on the effect of residual gas saturation. Pet. 4, 95–107.
- [29] Shamshiri, H., Jafarpour, B., 2010, November. Optimization of geologic CO2 storage in heterogeneous aquifers through improved sweep efficiency. In: SPE Int. Conf. on CO2 Capture, Storage, and Utilization, pp. SPE-139643. SPE.
- [30] Solomon, S., 2007. Climate Change 2007: The Physical Science Basis. Contribution of Working Group I to the Fourth Assessment Report of the Intergovernmental Panel on Climate Change. Cambridge University Press.
- [31] Storn, R., Price, K., 1997. Differential evolution A simple and efficient heuristic for global optimization over continuous spaces. J. Glob. Optim. 11, 341–359.
- [32] Szulczewski, M.L., MacMinn, C.W., Juanes, R., 2011. How pressure buildup and CO2 migration can both constrain storage capacity in deep saline aquifers. Energy Procedia 4, 4889–4896.
- [33] Voskov, D.V., Henley, H., Lucia, A., 2017. Fully compositional multi-scale reservoir simulation of various CO2 sequestration mechanisms. Comput. Chem. Eng. 96, 183–195.
- [34] Weir, G.J., White, S.P., Kissling, W.M., 1995. Reservoir storage and containment of greenhouse gases. Energy Convers. Manag. 36, 531–534.
- [35] Yamamoto, H., Doughty, C., 2011. Investigation of gridding effects for numerical simulations of CO2 geologic sequestration. Int. J. Greenh. Gas Control 5, 975–985.
- [36] Yang, X., 2010. Engineering Optimization: An Introduction with Metaheuristic Applications. John Wiley & Sons, Inc. ISBN: 9780470640425.
- [37] Yeten, B., Durlofsky, L.J., Aziz, K., 2002. Optimization of smart well control. In: Proc. SPE Int. Thermal Operations and Heavy Oil Symp. and Int. Horizontal Well Tech. Conf., Calgary, Canada, 4–7 November 2002.
- [38] You, J., Ampomah, W., Sun, Q., Kutsienyo, E.J., Balch, R.S., Dai, Z., Zhang, X., 2020. Machine learning based co-optimization of carbon dioxide sequestration and oil recovery in CO2-EOR project. J. Clean. Prod. 260, 120866.
- [39] Zhang, Y., Sahinidis, N.V., 2013. Developing Surrogate Models for CO2 Sequestration Using Polynomial Chaos Expansion; NRAP-TRS-III-004-2013; NRAP Technical Report Series; U.S. Department of Energy, National Energy Technology Laboratory: Morgantown, WV, 2013; p 20. DOI: 10.18141/1432683.
- [40] Zhang, Z., Agarwal, R.K., 2012. Numerical simulation and optimization of CO2 sequestration in saline aquifers for vertical and horizontal well injection. Comput. Geosci. 16, 891–899.
- [41] Zou, A., Durlofsky, L.J., 2023. Integrated framework for constrained optimization of horizontal/deviated well placement and control for geological CO2 storage. SPE J. 28, 2462–2481.